Convection-enhanced delivery of maghemite nanoparticles: Increased efficacy and MRI monitoring

Benny Perlstein, Zvi Ram, Dianne Daniels, Aharon Ocherashvilli, Yiftach Roth, Shlomo Margel, and Yael Mardor

Department of Chemistry, Bar-Ilan University, Ramat-Gan (B.P., S.M.); Department of Neurosurgery, Tel-Aviv Medical Center, Tel-Aviv (Z.R.); Advanced Technology Center, Sheba Medical Center, Tel-Hashomer, Ramat-Gan (D.D., A.O., Y.R., Y.M.); Israel

Convection-enhanced drug delivery (CED) is a novel approach to delivering drugs into brain tissue. Drugs are delivered continuously via a catheter, enabling large volume distributions of high drug concentrations with minimum systemic toxicity. Previously we demonstrated that CED formation/extent of small molecules may be significantly improved by increasing infusate viscosities. In this study we show that the same methodology can be applied to monodispersed maghemite nanoparticles (MNPs). For this purpose we used a normal rat brain model and performed CED of MNPs over short infusion times. By adding 3% sucrose or 3%–6% polyethylene glycol (PEG; molecular weight 400) to saline containing pristine MNPs, we increased infusate viscosity and obtained increased CED efficacy. Further, we show that CED of dextran-coated MNPs (dextran-MNPs) resulted in increased efficacy over pristine MNPs ($p < 0.007$). To establish the use of MRI for reliable depiction of MNP distribution, CED of fluorescent dextran-MNPs was performed, demonstrating a significant correlation between the distributions as depicted by MRI and spectroscopic images ($r^2 = 0.74$, $p < 0.0002$). MRI follow-up showed that approximately 80%–90% of the dextran-MNPs were cleared from the rat brain within 40 days of CED; the rest remained in the brain for more than 4 months. MNPs have been tested for applications such as targeted drug delivery and controlled drug release and are clinically used as a contrast agent for MRI. Thus, combining the CED method with the advantages of MNPs may provide a powerful tool to treat and monitor brain tumors. *Neuro-Oncology 10, 153–161, 2008 (Posted to Neuro-Oncology [serial online], Doc. D07-00078, March 3, 2008. URL http://neuro-oncology.dukejournals.org; DOI: 10.1215/15228517-2008-002)*

Keywords: brain tumors, convection-enhanced drug delivery, drug delivery, magnetic resonance imaging, nanoparticles

One of the most promising methods for efficient drug delivery into brain tumors is convection-enhanced drug delivery (CED). CED involves positioning the tip of an infusion catheter within the brain tissue and supplying the drug through the catheter while maintaining a positive pressure gradient from the tip of the catheter during infusion. The catheter is connected to a pump that delivers the drug and maintains the desired pressure gradient throughout delivery. Drug delivery rates are typically about 0.5–4.0 μl/min with infusion distances on the order of centimeters. CED involves formation of pressure gradients in the tissue. Convective pressure occurs under normal conditions of bulk flow of brain interstitial fluid due to changes in hydrostatic and osmotic pressures,[1] under the pathologic conditions of vasogenic edema,[2] which involves an increase in extracellular fluid volume, and after direct infusion of solutions into the brain parenchyma.[3] CED

Received April 22, 2007; accepted October 17, 2007.

Address correspondence to Yael Mardor, Chief Scientist, Advanced Technology Center Sheba Medical Center, Tel-Hashomer, 52621, Israel (yael.mardor@sheba.health.gov.il).

supplements diffusion and greatly enhances the distribution of molecules in the brain,[4,5] capable of obtaining in situ drug concentrations several orders of magnitude greater than those obtained by systemic administration. The concentration profile is relatively flat up to the flow front.[6]

We have recently published the results of a phase I/II clinical trial where recurrent glioblastoma multiforme patients received CED of Taxol with a significant antitumor response rate.[7] CED of other drugs such as Tf-CRM107,[8] TP-38,[9] and PE38KDEL[10] was also found to have clinical activity of varying degrees. Furthermore, recent animal studies show that liposomes can be delivered via CED into brain and brain tumors, as a vehicle for therapeutic agent delivery.[11–14]

Accumulated clinical experience shows that there is significant variability in the extent of convection among drugs and among patients. For that reason, a reliable real-time, noninvasive monitoring technique is required, as well as means to increase CED efficacy. We have recently shown that low-viscosity infusates tend to backflow along the catheter track while high-viscosity infusates tend to form efficient convection.[15] We also showed that CED formation and extent may be improved by increasing infusate viscosities, thus increasing treatment effects. In this study we used our novel high-viscosity methods to obtain efficient CED of maghemite nanoparticles (MNPs) of approximately 80 nm average diameter, which can be directly depicted by MRI, in a normal rat brain model.

Magnetic nanoparticles are considered to be spherical particles with magnetic properties, ranging from a few nanometers to approximately 100 nm in size. These particles, because of their spherical shape, very large surface area, and magnetic properties, may have a wide range of potential applications, such as drug delivery, MRI, specific cell labeling and separation, cell tracking, diagnostics, hyperthermia, and biocatalysis.[16–22] In recent years, extensive efforts have been made to design nanoparticles for specific drug targeting applications.[23–27] Of particular interest for the present study is the use of magnetic nanoparticles for specific targeting via MRI. Recently, we have prepared and characterized new uniform maghemite (γ-Fe_2O_3) nanoparticles. These MNPs are formed by controlled nucleation and then growth of thin maghemite films onto appropriate nuclei.[17,28] The resulting nanoparticles are superparamagnetic, biodegradable, and nontoxic, and have a narrow size distribution. Due to the superparamagnetic properties, it is possible to perform the imaging and assessment of the MNP distribution using MRI. Superparamagnetic MNPs produce a dramatic long-range disturbance in magnetic field homogeneity, causing marked shortening of T2* relaxation time. (T2* is the characteristic time constant that describes the decay of transverse magnetization, taking into account the inhomogeneity in static magnetic fields and the spin-spin relaxation time.) This results in a rapid loss of phase coherence and loss of MRI signal in the area of the particles. The goals of this study were (1) to establish the use of MRI for a reliable depiction of the MNP distribution in a normal rat brain model; (2) to use MRI to optimize infusate viscosity parameters to obtain maximum MNP distribution in minimum infusion time; and (3) to study the clearance time of MNPs from brain tissue for future use in sustained drug release.

Materials and Methods

Materials

Gelatin (type A from porcine skin, 300 bloom), dextran (molecular weight [MW] 35,000–45,000), divinyl sulfone (DVS), glycine, sucrose, and polyethylene glycol (PEG) (MW 400) were all purchased from Sigma (Rehovot, Israel). Salts for buffers were purchased from Bio-Lab Ltd. (Jerusalem, Israel). Formaldehyde was purchased from Gadot Biochemical Industries, Ltd. (Haifa Bay, Israel). Water was purified by passing deionized water through an Elgastat Spectrum reverse osmosis system (Elga Ltd., High Wycombe, UK).

Experimental Design

Three types of MNPs were prepared: (1) pristine MNPs; (2) MNPs coated with dextran (dextran-MNPs); and (3) fluorescent dextran-MNPs. These MNPs were mixed in various solutions containing saline or 3% or 6% PEG (MW 400) in saline or 3% sucrose in saline. Relative viscosity was measured in an Ostwald-type viscometer relative to saline solution at 20°C. The MNP solutions were infused into the striatum of normal Sprague-Dawley (SD) rats (males, 250–300 g). MRI and spectroscopic imaging methods were used to assess the MNP distribution in the brain. For spectroscopic imaging, brains were harvested and submerged in formaldehyde for 24 h and then sliced at the site of the injection. The study was performed in accordance with the guidelines of the Animal Care and Use Committee of Sheba Medical Center, which is recognized by the Israeli authorities for animal experimentation.

Preparation of MNPs

MNPs of narrow size distribution were prepared by nucleation followed by controlled growth of magnetic iron oxide layers onto gelatin nuclei, as described previously.[17,28] Briefly, $FeCl_2$ solution (10 mmol/5 ml 0.01 normal [N] HCl) was added to 80-ml aqueous solution containing 200 mg porcine gelatin, followed by $NaNO_2$ solution (7 mmol/5 ml H_2O). After a reaction time of 10 min, the pH was raised to 9.5 by adding NaOH aqueous solution (1 N). This procedure was repeated four more times. The MNPs were then washed from excess reagents using magnetic columns. Dextran coating was performed by shaking the aqueous suspension of the MNPs containing 2% dextran (MW 35,000–45,000) at 85°C for 1 h. The dextran-coated MNPs were then washed by means of magnetic columns. In order to prevent leakage of dextran from the nanoparticles' surface to the aqueous continuous phase, crosslinking of the adsorbed dextran with DVS was performed

by shaking the dextran-MNPs (2.5 mg/ml) with DVS ([MNP]/[DVS] = 1 mg/4.3 μl) at pH 10.5 and 60°C. The dextran-MNPs were then washed with bicarbonate buffer (0.1 M, pH 8.3) using magnetic columns. The remaining residual activated double bonds of the DVS were then blocked with 1% glycine aqueous solution. Excess glycine was washed from the obtained dextran-MNPs using magnetic columns and saline. Fluorescent dextran-MNPs were prepared similarly, by adding rhodamine molecules to the gelatin solution, thereby entrapping the rhodamine within the MNP.

MNP Characterization

The diameter and size distribution of the MNPs were measured by a submicron particle analyzer (N4MD, Coulter Electronics Ltd., Hialeah, FL, USA) and a transmission electron microscope (TEM) (JEM-1200EX, JEOL, Japan). Magnetic measurements were performed on a sample of dextran-MNPs that was introduced into a plastic capsule. Measurements at room temperature were performed using an Oxford Instrument vibrating sample magnetometer (VSM). Magnetization was measured as a function of the external field being swept up and down (–16,000 oersteds [Oe] $< H_{applied} <$ 16,000 Oe, in steps of 200 Oe).

CED Procedure

Under full anesthesia, a midline scalp incision was made to identify the bregma. A 1-mm burr hole was made in the right region of the skull, 2 mm lateral and 3 mm anterior to the bregma. A 33-gauge needle attached to a 1,000-μl syringe (Gastight, Hamilton Co., Reno, NV, USA) was placed stereotactically 6 mm deep in the rat striatum. In order to increase the sensitivity of the test, we introduced challenging CED conditions by inserting the injector needle only 4.5 mm into the rat striatum. The infusion was performed using a BASI syringe pump (Bioanalytical Systems, Inc., West Lafayette, IN, USA) at a rate of 4 μl/min for 15 min (unless stated otherwise).

Imaging Protocol

T2*-weighted MR images were acquired immediately after the convection treatment using a 0.5-T interventional GE MRI system and a dedicated, specially designed animal coil. T2*-weighted images were acquired with 3-mm slices, no gap, 14 × 10.5-cm^2 field of view, a gradient echo (GRE) sequence with a 256 × 256 matrix, repetition time (TR) = 350 ms, echo time (TE) = 14.5 ms, flip angle = 60°, and two signal averages. Spectral images were obtained with the SD300 system based on Fourier transform (FT) spectroscopy (Applied Spectral Imaging [ASI], Migdal Ha'Emek, Israel). The spectral images were analyzed off-line with dedicated ASI-developed software. The principle of spectral imaging, combining conventional imaging with FT spectroscopy, has been described elsewhere.[29] An excitation filter of 550 ± 20 nm and an emission filter of >600 nm were used for rhodamine fluorescence detection.

Calculation of MNP Distribution Area

The area (in mm^2) of infusate distribution was calculated from the T2*-weighted MR images acquired immediately after CED treatment. Regions of interest (ROIs) were defined over the entire signal void region in each slice (excluding the ventricles). The number of pixels in the ROIs were counted and multiplied by the area of a single pixel. Data are presented as average ± SD. The differences in ROI sizes were analyzed using the nonparametric Wilcoxon two-sample test. Significant differences between the groups were considered when the calculated p value was ≤ 0.05.

In the case of fluorescent dextran-MNP infusate, the ROIs were also calculated from the spectroscopic images, and a correlation between the ROI sizes derived from the two imaging methodologies was calculated using Pearson's correlation test.

Prussian Blue Staining of Extracted Brains

Prussian blue staining (Diagnostic BioSystems, Pleasanton, CA, USA) was performed to demonstrate dextran-MNP microdistribution in the rat striatum (dextran-MNPs stained blue). Briefly, 23 days after dextran-MNP convection, the brains were extracted and fixed in 4% glutaraldehyde for 48 h. The brains were paraffin embedded, and 5-μm slices were chosen from the site of convection. The slices were deparaffinized and placed in a Prussian blue solution for 20 min, and then in a nuclear fast red solution, which stained the nuclei red and other tissue pink. Photographs were acquired with a charge-coupled device (CCD) digital camera connected to a light microscope (Olympus BX60, Olympus, Tokyo, Japan).

Results

Characterization of MNPs

The mean diameter of the dextran-MNPs as measured by TEM was 14 ± 4 nm. An example of a TEM photomicrograph is shown in Fig. 1A. The light scattering measurements (Fig. 1B) of the dextran-MNPs dispersed in saline resulted in an average diameter of about 81 ± 9 nm with no observable aggregates. A hysteresis loop at room temperature of the dextran-MNPs is shown in Fig. 1C. Similar results were obtained for pristine MNPs (data not shown).

Efficient CED of Dextran-MNPs into the Rat Striatum

Dextran-MNPs (0.2 mg/ml) were infused at a rate of 4 μl/min for 15 min into the striatum of 31 rats. Rats were scanned by MRI immediately after treatment (Fig. 2). Efficient CED was depicted as homogeneous signal loss throughout the striatum. Inefficient CED, caused by backflow of the infusate along the catheter path, resulted in release into the ventricular system, and was depicted as accumulation of signal loss in the ventricles. The aver-

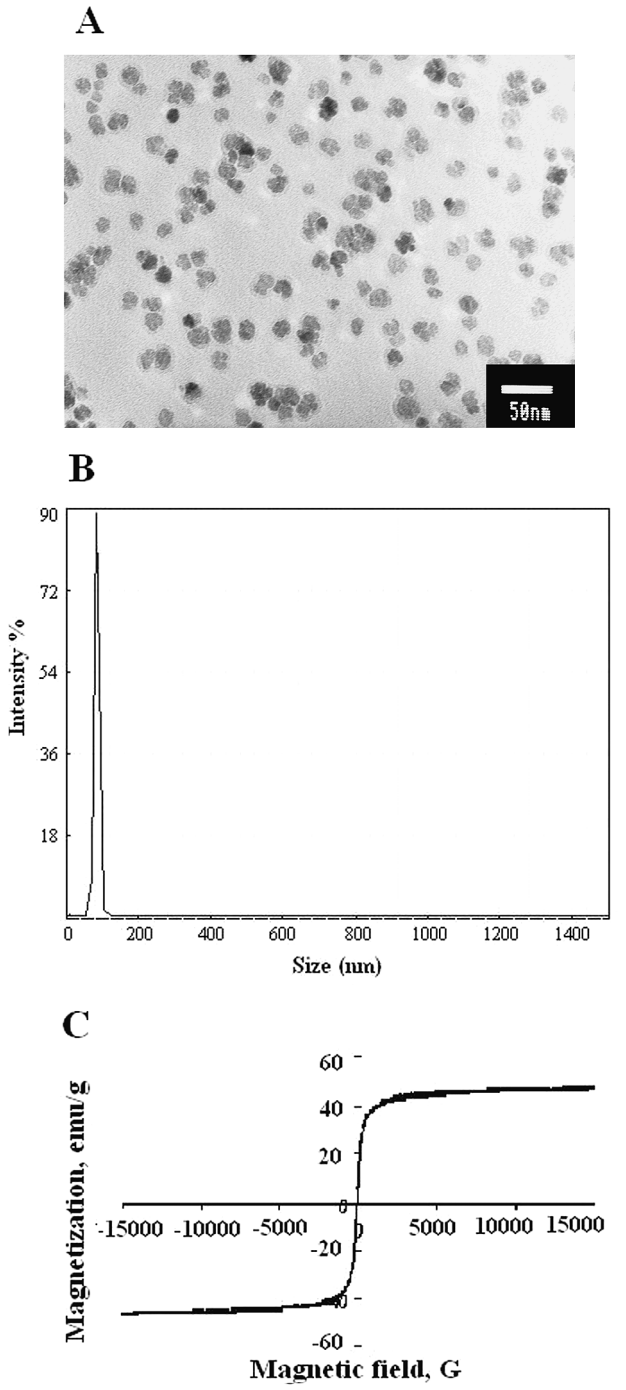

Fig. 1. Monodispersed maghemite nanoparticle (MNP) characterization: (A) transmission electron microscope photomicrograph of dextran-MNPs; (B) graph demonstrating average diameter of dextran-MNPs dispersed in water; (C) room temperature magnetization vibrating sample magnetometer loops of dextran-MNPs.

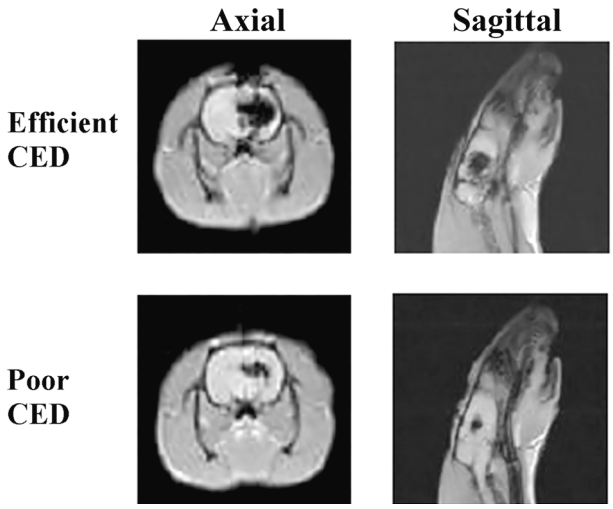

Fig. 2. Convection-enhanced drug delivery (CED) of dextran-coated monodispersed maghemite nanoparticles (dextran-MNPs) into a rat striatum: axial and sagittal slices of T2*-weighted gradient echo MRI acquired immediately after treatment with a 0.2 mg/ml infusate at 4 μl/min over 15 min. Examples of poor CED (lower panel) versus efficient CED (upper panel) are shown. The presence of dextran-MNPs is depicted in the gradient echo MR images as a signal-void region near the catheter tip location.

age area of the signal void induced by the dextran-MNP distribution was 25.4 ± 8.1 mm^2 (median = 24.5 mm^2, range = 6.0–42.4 mm^2).

Clearance of Dextran-MNPs from Rat Brain

In order to study the clearance rate, we infused dextran-MNPs (0.2 mg/ml) at a rate of 4 μl/min for 15 min into the striatum of 11 rats. The clearance rate was regularly monitored by MRI until most of the dextran-MNPs were cleared from the brain (Fig. 3). Data show a close to linear rate down to approximately 80%–90% clearance after 40 days, at which a plateau is reached.

Prussian blue staining of brains extracted 23 days after treatment showed that most of the residual MNPs were located either intracellularly or adjacent to the cell surfaces. Examples are shown in Fig. 4.

Direct Visualization of MNP Distribution with a High Concentration Infusate

In order to visualize the MNP distribution in the brain directly, we infused a high concentration (2 mg/ml) of dextran-MNPs, resulting in a clear depiction of the treated region (Fig. 5).

Correlation between Spectroscopic and MR Imaging of Fluorescent Dextran-MNP Distribution

To establish the use of MRI for reliable depiction of the dextran-MNP distribution in the rat brain, we used fluorescent dextran-MNPs (0.2 mg/ml) dispersed in

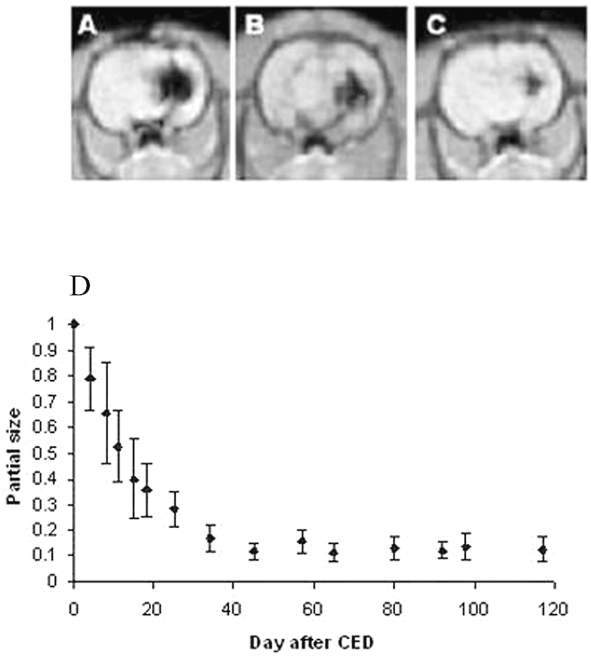

Fig. 3. Clearance of dextran-coated monodispersed maghemite nanoparticles (dextran-MNPs) from the striatum over time. Dextran-MNPs (0.2 mg/ml) were infused at 4 μl/min over 15 min into the rat striatum. Examples show axial T2*-weighted gradient echo MR images acquired (A) immediately, (B) 3 days, and (C) 27 days after convection-enhanced drug delivery (CED) treatment of one rat. The MNP area of distribution, normalized to the initial distribution area (calculated from the images acquired immediately after treatment), as a function of time is shown in (D). The average number of animals for each time point was 4.6.

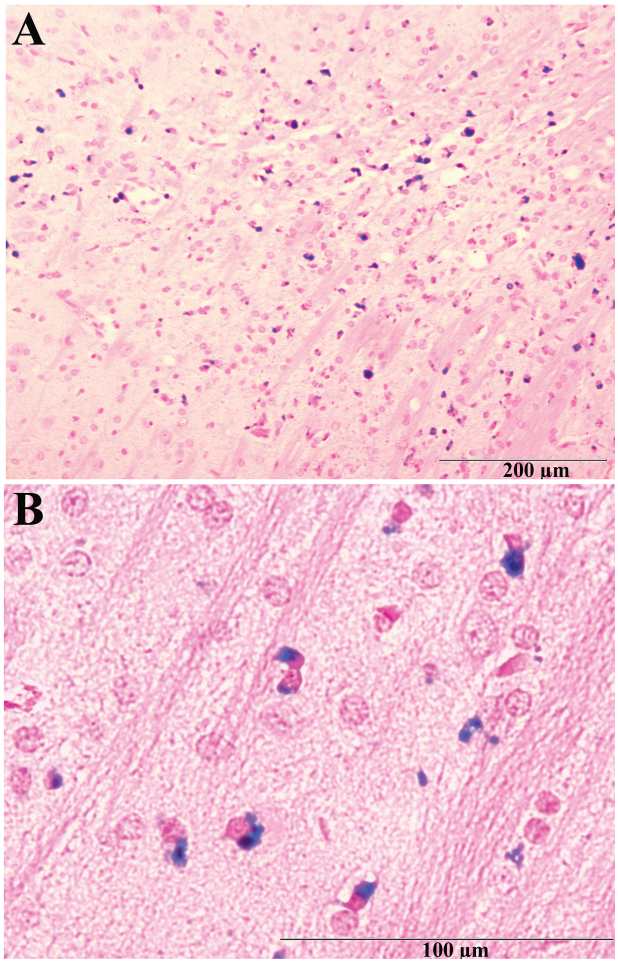

Fig. 4. Location of dextran-coated monodispersed maghemite nanoparticles (dextran-MNPs) within the striatum 23 days after convection-enhanced drug delivery (CED): light microscope photographs of the rat brain striatum 23 days after CED with dextran-MNPs. Slices were chosen from the site of CED and stained with Prussian blue to visualize the microlocation of dextran-MNPs. Blue color indicates the presence of dextran-MNPs. Slides were counterstained with nuclear fast red, which stained nuclei red and other tissue pink.

saline. These fluorescent dextran-MNPs were infused at a rate of 4 μl/min for 15 min into the striatum of 12 rats (Fig. 6). The fluorescent dextran-MNP distribution areas in the striatum, as depicted by the MR images and the spectroscopic images, were calculated. The correlation (Pearson's correlation; $r^2 = 0.74$, $p < 0.0002$) between these two imaging methodologies (Fig. 6) was found to be significant, thus establishing the validity of MRI for monitoring CED of MNPs at the given concentration.

CED Efficacy of Pristine MNPs versus Dextran-MNPs

In order to increase the sensitivity of the test, we introduced challenging CED conditions (see Materials and Methods section). The rats were divided into two groups of seven each. One group underwent CED with pristine MNPs (0.2 mg/ml) while the other group underwent CED with dextran-MNPs (0.2 mg/ml). The average area of distribution (calculated from the MR images) of pristine MNPs and dextran-MNPs was 13.4 ± 6.1 mm^2 (median = 12.2 mm^2, range = 4.9–22.2 mm^2) and 23.9 ± 4.6 mm^2 (median = 25.9 mm^2, range = 16.6–29.7 mm^2), respectively. The dextran-MNP distribution area was significantly larger than that of the pristine MNPs ($p < 0.007$).

Increasing the Viscosity of the MNP Solution Improves CED Efficacy

Using the challenging CED conditions, we examined the change in CED area distribution caused by increased viscosity infusates. For that purpose, two suspensions of pristine MNPs were prepared. One consisted of MNPs suspended in saline (0.2 mg/ml, relative viscosity = 1.00 ± 0.03), and the other consisted of MNPs suspended in 3% sucrose in saline (0.2 mg/ml, relative viscosity = 1.09 ± 0.03). The rats were divided into two groups. Each group received only one of the MNP suspensions. Infusion into the rat striatum was performed at a rate of 4 μl/min for a duration of 15 min. The rats were scanned by MRI immediately after treatment. The calculated distribution areas of MNPs in saline and MNPs

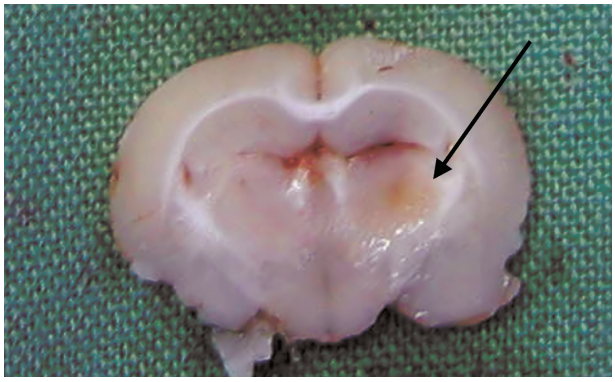

Fig. 5. Convection-enhanced drug delivery (CED) of high concentration of dextran-coated monodispersed maghemite nanoparticles (dextran-MNPs), demonstrating direct visualization of MNP distribution in the brain. The brain was harvested immediately after treatment with a high-concentration infusate (2 mg/ml). The arrow points to the brown area in the right hemisphere, which indicates the presence of dextran-MNPs.

in 3% sucrose solution were 13.4 ± 6.1 mm^2 (median = 12.2 mm^2, range = 4.9–22.2 mm^2) and 23 ± 3.4 mm^2 (median = 23.2, range = 17.2–28.2 mm^2), respectively, with a significantly larger area for MNPs in 3% sucrose ($p < 0.007$). In order to further study the influence of increased viscosity on the CED distribution area of pristine MNPs, we infused a solution of pristine MNPs (0.2 mg/ml) in 3% or 6% PEG (relative viscosity, 1.112 ± 0.028 and 1.252 ± 0.031, respectively). The resulting distribution areas, as calculated from the MRI, were compared with those of pristine MNPs in saline (Fig. 7). The distribution areas of pristine MNPs in saline and 3% and 6% PEG solutions were 17.9 ± 6.8 mm^2 (median = 18.0 mm^2, range = 4.2–24.8 mm^2), 24.0 ± 4.7 mm^2 (median = 24.9 mm^2, range = 14.6–28.9 mm^2), and 24.7 ± 3.0 mm^2 (median = 25.5, range = 19.6–29.0 mm^2), respectively. CED extent of pristine MNPs in 3% PEG and 6% PEG was significantly larger than that of pristine MNPs in saline ($p < 0.053$ and $p < 0.011$, respectively).

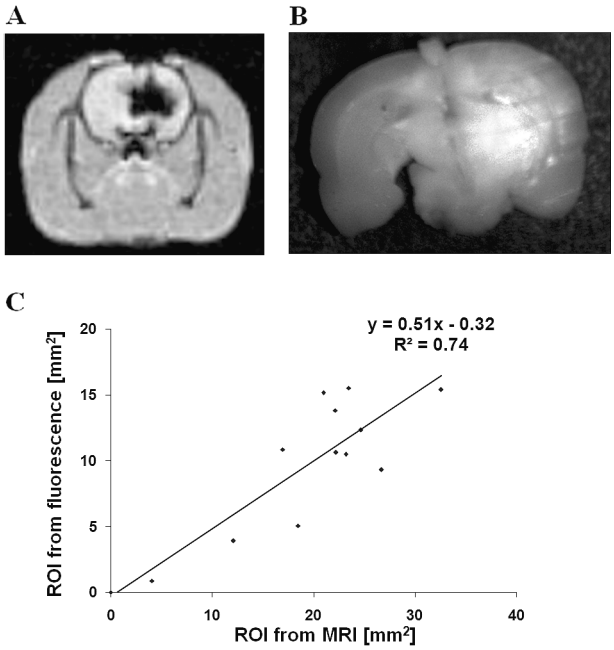

Fig. 6. Spectroscopic and MR imaging of fluorescent monodispersed maghemite nanoparticles (dextran-MNPs): (A) axial slice of T2*-weighted gradient echo MRI acquired immediately after convection-enhanced drug delivery (CED) treatment with a 0.2 mg/ml infusate at 4 μl/min over 15 min; (B) spectroscopic image of a slice from the same rat brain after fixation with formaldehyde; (C) correlation between the fluorescent dextran-MNP distribution area (mm^2) as depicted by spectroscopic and imaging MRI.

Discussion

This study demonstrates the feasibility of obtaining efficient CED of MNPs in a normal rat brain model. The dextran-MNP particle size as measured by TEM was 14 ± 4 nm. In contrast, light scattering measurements showed a size of 81 ± 9 nm. These differences are attributed to the fact that TEM measures the dry diameter, while light scattering determines the hydrodynamic diameter, which takes the hydrated layers on the particle's surface into account. Furthermore, we show that the $M(H)$ curve of dextran-MNP does not saturate at 10,000 Oe, and that the obtained magnetic moment at 10,000 Oe is about 41 electromagnetic units [emu] g^{-1}. In addition, the $M(H)$ curve does not exhibit any coercivity. Both features are typical of superparamagnetic behavior.

The results show that efficient CED into rat striatum could be obtained with short infusion times (15 min) of dextran-MNPs dispersed in saline. By introducing more challenging CED conditions, thus simulating better actual clinical conditions, we increased the sensitivity of the experiment to the infusate/MNP characteristics. By applying these conditions, we showed that coating the MNPs with dextran increased the distribution area obtained by CED. One explanation for this observation may be the effect of surface coating on protein adsorption. The steric brushes of the dextran macromolecules are believed to reduce interactions with proteins.[30,31] Thus, it may be that dextran-MNPs pass more easily through the tissue than do pristine MNPs. Indeed, it has been shown that coating of nanoparticles is essential for preventing nonspecific adsorption of plasma proteins. Biocompatible polymers such as dextran and PEG have been used for this purpose.[32–34]

Previously, we showed that low-viscosity infusates tend to backflow along the catheter track while high-viscosity infusates tend to form efficient convection. In addition, our previous results suggest that CED formation and extent may be significantly improved by increasing infusate viscosities, thus increasing treatment effects.[15] Indeed, by applying the more challenging CED conditions, we showed that the increased viscosity methodology could be applied to pristine MNPs and that it significantly improved the efficiency of CED.

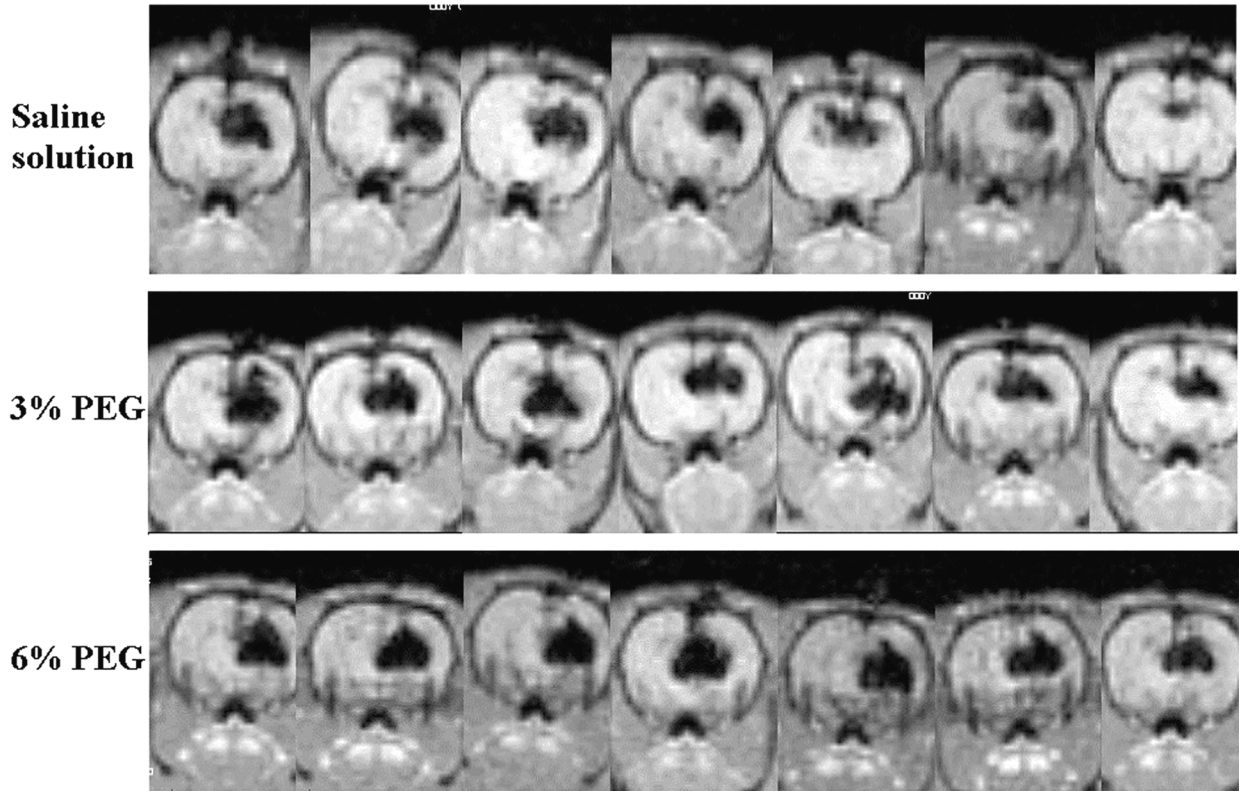

Fig. 7. Convection-enhanced drug delivery (CED) of dextran-coated monodispersed maghemite nanoparticles (MNPs) in high-viscosity medium of 3% or 6% polyethylene glycol (PEG): axial slices of T2*-weighted gradient echo MRIs of rat brains acquired immediately after CED of pristine MNPs in saline, 3% or 6% PEG ($n = 7$ for each group), with a 0.2 mg/ml infusate at 4 μl/min over 15 min. The MNP distribution area was significantly increased when MNPs were in 6% PEG solution ($p < 0.04$).

The long clearance time of dextran-MNPs from the rat brain tissue may be explained by the Prussian blue staining depicting the residual MNPs either intracellularly or adjacent to the cell surface. This suggests that the clearance observed in the first 30–40 days may be of extracellular MNPs. The long presence of the particles in the cell vicinity may suggest the use of MNPs as a vehicle for sustained drug release. The MNPs used in this study may be advantageous for in vivo use. No toxicity was detected up to 120 days after CED. In addition, the MNPs are biodegradable, have a narrow size distribution, and are stable at physiological pH.

In an earlier study[35] on CED of dextran-coated monocrystalline iron oxide nanocompounds (MION-46), Kroll et al. evaluated the effect of dose, volume of injection, and infusion time on CED volume during intracerebral CED. Our study demonstrates that other parameters, such as viscosity and surface coating, should also be taken into account since they significantly affect the distribution area of CED and allow for higher CED flow rates, thus shorter infusion times.

The correlation between the distributions as depicted by MRI and spectroscopic images establishes the use of MRI for reliable MNP imaging. However, calibration is still needed for different MNP concentrations, since the MRI artifacts caused by MNPs are strongly affected by MNP concentration. In this study, we used MNPs as a model to show the feasibility of obtaining efficient CED of large particles with our high-viscosity methodologies. The ability to convect large particles efficiently implies that it may be possible to efficiently convect other similar size particles such as gene-therapy–related products, liposomes, and so on. Indeed, it has been shown elsewhere that the volume of CED of adenovirus and MION-46 did not significantly differ in a rat brain model.[36]

Initial clinical experience shows that there is significant variability in the efficient formation and extent of convection among patients, as well as among drugs. Careful examination of the radiological clinical data points to backflow along the catheter path or leakage into low-density regions as one of the main obstacles in forming efficient convection clinically.

We have shown that high-viscosity infusates reduce the sensitivity to backflow, thus increasing the probability for forming efficient convection.[15] These results were consistent with the exceptionally high CED efficacy observed in clinical studies with CED of Taxol.[7,37] As far as the authors are aware, Taxol is the highest viscosity infusate used in clinical CED-based trials, and the observed response rates were exceptionally high.

The results presented in this article are an extension of the previous study, which dealt with small molecules,

suggesting that high viscosity may increase CED efficacy of large particles, MNPs, as well.

The application of CED together with MNPs may enable the use of drugs and/or drug carriers that have been considered inappropriate for convection treatment of brain tumors. The use of MNPs as a drug carrier may enable the delivery of large therapeutic agents and targeted drug delivery. In addition, the long clearance time of MNPs may enable slow drug release.

Acknowledgments

We thank Dr. Tammy Lublin-Tennenbaum for her help in the synthesis and characterization of MNPs. Thanks also to Mr. Gregory Tamar for his help in performing the CED procedure in the animals, to Dr. Genady Kostenich for his help in performing the spectroscopic imaging, and to Mrs. Sharona Salomon for handling the infusates.

References

1. Rosenberg GA, Kyner WT, Estrada E. Bulk flow of brain interstitial fluid under normal and hyperosmolar conditions. *Am J Physiol Renal Physiol*. 1980;238:F42–F49.
2. Reulen HJ, Graham R, Spatz M, Klatzo I. Role of pressure gradients and bulk flow in dynamics of vasogenic brain edema. *J Neurosurg*. 1977;46:24–35.
3. Ohata K, Marmarou A. Clearance of brain edema and macromolecules through the cortical extracellular space. *J Neurosurg*. 1992;77:387–396.
4. Bobo RH, Laske DW, Akbasak AI, Morrison PF, Dedrick RL, Oldfield EH. Convection-enhanced delivery of macromolecules in the brain. *PNAS*. 1994;91:2076–2080.
5. Lieberman DM, Laske DW, Morrison PF, Bankiewicz KS, Oldfield EH. Convection-enhanced distribution of large molecules in gray matter during interstitial drug infusion. *J Neurosurg*. 1995;82:1021–1029.
6. Morrison PF, Laske DW, Bobo H, Oldfield EH, Dedrick RL. High-flow microinfusion: tissue penetration and pharmacodynamics. *Am J Physiol Regul Integr Comp Physiol*. 1994;266:R292–R305.
7. Lidar Z, Mardor Y, Jonas T, et al. Convection-enhanced delivery of paclitaxel for the treatment of recurrent malignant glioma: a phase I/II clinical study. *J Neurosurg*. 2004;100:472–479.
8. Weaver M, Laske DW. Transferrin receptor ligand-targeted toxin conjugate (Tf-CRM107) for therapy of malignant gliomas. *J Neurooncol*. 2003;65:3–14.
9. Sampson JH, Akabani G, Archer GE et al. Progress report of a phase I study of the intracerebral microinfusion of a recombinant chimeric protein composed of transforming growth factor (TGF)-α and a mutated form of the *Pseudomonas* exotoxin termed PE-38 (TP-38) for the treatment of malignant brain tumors. *J Neurooncol*. 2003;65:27–35.
10. Kawakami M, Kawakami K, Puri RK. Interleukin-4–*Pseudomonas* exotoxin chimeric fusion protein for malignant glioma therapy. *J Neurooncol*. 2003;65:15–25.
11. Mamot C, Nguyen BJ, Pourdehnad M, et al. Extensive distribution of liposomes in rodent brains and brain tumors following convection-enhanced delivery. *J Neurooncol*. 2004;68:1–9.
12. Saito R, Bringas JR, McKnight TR, et al. Distribution of liposomes into brain and rat brain tumor models by convection-enhanced delivery monitored with magnetic resonance imaging. *Cancer Res*. 2004;64:2572–2579.
13. Krauzea TM, Mcknightc RT, Yamashitaa Y, et al. Real-time visualization and characterization of liposomal delivery into the monkey brain by magnetic resonance imaging. *Brain Res Prot*. 2005;16:20–26.
14. Saito R, Krauzea TM, Bringas RJ, et al. Gadolinium-loaded liposomes allow for real-time magnetic resonance imaging of convection-enhanced delivery in the primate brain. *Exp Neurol*. 2005;196:381–389.
15. Mardor Y, Rahav O, Zauberman Y, et al. Convection-enhanced drug delivery: increased efficacy and magnetic resonance image monitoring. *Cancer Res*. 2005;65:6858–6863.
16. Minjuan Z, Qun Z, Itoh T, Abe M. Ferrite plating on porous silica microspheres for ultrasonic contrast agents. *IEEE Trans Magn*. 1994;30:4692–4694.
17. Hergt R, Hiergeist R, Hilger I, et al. Maghemite nanoparticles with very high AC-losses for application in RF-magnetic hyperthermia. *J Magn Magn Mater*. 2004;270:345–357.
18. Pankhurst QA, Connolly J, Jones SK, Dobson J. Applications of magnetic nanoparticles in biomedicine. *J Phys D Appl Phys*. 2003;36:R167–R181.
19. Arbab AS, Yocum GT, Kalish H, et al. Efficient magnetic cell labeling with protamine sulfate complexed to ferumoxides for cellular MRI. *Blood*. 2004;104:1217–1223.
20. Lewin M, Carlesso N, Tung C-H, et al. Tat peptide-derivatized magnetic nanoparticles allow in vivo tracking and recovery of progenitor cells. *Nat Biotech*. 2000;18:410–414.
21. Rogers JW, Meyer HC, Kramer MC. Technology Insight: in vivo cell tracking by use of MRI. *Nat Clin Pract Cardiovasc Med*. 2006;3:554–562.
22. Margel S, Burdygin I, Reznikov V, et al. Functional nanoparticles: synthesis and biological applications. *Recent Res Dev Polym Sci*. 1997;1:51–78.
23. Green-Sadana T, Kuttnera Y, Lublin-Tennenbaumb T, et al. Glial cell line-derived neurotrophic factor-conjugated nanoparticles suppress acquisition of cocaine self-administration in rats. *Exp Neurol*. 2005;194:97–105.
24. Farokhzad OC, Jon S, Khademhosseini A, et al. Nanoparticle-aptamer bioconjugates: a new approach for targeting prostate cancer cells. *Cancer Res*. 2004;64:7668–7672.
25. Schroeder U, Sommerfeld P, Ulrich S, Sabel AB. Nanoparticle technology for delivery of drugs across the blood-brain barrier. *J Pharm Sci*. 1998;87:1305–1307.
26. Park EK, Lee SB, Lee YM. Preparation and characterization of methoxy poly(ethylene glycol)/poly([var epsilon]-caprolactone) amphiphilic block copolymeric nanospheres for tumor-specific folate-mediated targeting of anticancer drugs. *Biomaterials*. 2005;26:1053–1061.
27. Kreuter J. Nanoparticulate systems for brain delivery of drugs. *Adv Drug Deliv Rev*. 2001;47:65–81.
28. Margel S, Gura S. Nucleation and growth of magnetic metal oxide nanoparticles and its use. Israel patent WO9962079. 1999-12-02.

29. Kostenich G, Kimel S, Peled S, Orenstein A. Monitoring PDT-induced damage using spectrally resolved reflectance imaging of tissue oxygenation. *Cancer Lett.* 2005;219:169–175.
30. Moghimi SM, Hunter AC, Murray JC. Long-circulating and target-specific nanoparticles: theory to practice. *Pharmacol Rev.* 2001;53:283–318.
31. Pain D, Das PK, Ghosh P, Bachhawat K. Increased circulatory half-life of liposomes after conjunction with dextran. *J Biosci.* 1984;6(6):811–816.
32. Berry CC, Wells S, Charles S, Curtis ASG. Dextran and albumin derivatised iron oxide nanoparticles: influence on fibroblasts in vitro. *Biomaterials.* 2003;24:4551–4557.
33. Weissleder R, Bogdanov A, Neuwelt EA, Papisov M. Long-circulating iron oxides for MR imaging. *Adv Drug Deliv Rev.* 1995;16:321–334.
34. Lemarchand C, Gref R, Passirani C, et al. Influence of polysaccharide coating on the interactions of nanoparticles with biological systems. *Biomaterials.* 2006;27:108–118.
35. Kroll RA, Michael A, Muldoon LL, Roman-Goldstein S, Neuwelt EA. Increasing volume of distribution to the brain with interstitial infusion: dose, rather than convection, night be the most important factor. *Neurosurg Online.* 1996;38:746–754.
36. Muldoon LL, Nilaver G, Kroll RA, et al. Comparison of intracerebral inoculation and osmotic blood-brain barrier disruption for delivery of adenovirus, herpesvirus, and iron oxide particles to normal rat brain. *Am J Pathol.* 1995;147:1840–1851.
37. Pöpperl G, Goldbrunner R, Gildehaus FJ, et al. O-(2–[18F]fluoroethyl)-L-tyrosine PET for monitoring the effects of convection-enhanced delivery of paclitaxel in patients with recurrent glioblastoma. *Eur J Nucl Med Mol Imaging.* 2005; 32: 1018–1025.